Two multi-temporal datasets to track the enhanced landsliding after the 2008 Wenchuan earthquake

Xuanmei Fan[1], Gianvito Scaringi[1], Fan Yang[1], Guillem Domènech[1], Xiaojun Guo[2], Lanxin Dai[1], Chaoyang He[1], Qiang Xu[1], Runqiu Huang[1]

5 [1]State Key Laboratory of Geohazard Prevention and Geoenvironment Protection, Chengdu University of Technology, Chengdu, 610059, China
[2]Key Laboratory of Mountain Hazards and Surface Process, Institute of Mountain Hazards and Environment, Chinese Academy of Sciences, Chengdu, 610041, China

Correspondence to: Xuanmei Fan (fxm_cdut@qq.com), Xiaojun Guo (aaronguo@imde.ac.cn) and Qiang Xu (xq-68@qq.com)

10 **Abstract.** We release two datasets that track the enhanced landsliding induced by the M_w 7.9 2008 Wenchuan earthquake over a portion of the Longmen mountains, at the eastern margin of the Tibetan plateau (Sichuan, China). The first dataset is a geo-referenced multi-temporal polygon-based inventory of pre- and coseismic landslides, post-seismic remobilisations of coseismic landslide debris, and post-seismic landslides (new failures). The inventory covers 462.5 km^2 in the earthquake's epicentral area, from 2005 to 2015. The second dataset records the debris flows that occurred from 2008 to 2017 in a larger

15 area (~17,000 km^2), together with information on their triggering rainfalls recorded by a network of rain gauges. For some well-monitored event, we provide detailed information on rainfall, discharge, flow depth and density. The datasets can be used to analyse, at various scales, the patterns of enhanced landsliding caused by the earthquake. They can be compared to inventories relative to past or new earthquakes or other triggers to reveal common or distinctive controlling factors. To our knowledge, no other inventories that track the temporal evolution of earthquake-induced mass wasting have been made freely

20 available thus far. Our datasets are available at https://doi.org/10.5281/zenodo.1405490. We also encourage other researchers to share their datasets to facilitate research on post-seismic geological hazards.

1 Introduction

1.1 Earthquake-induced enhanced landsliding

Large earthquakes cause major disturbances to the patterns of erosion and sediment export from mountain belts (e.g.,

25 Keefer, 1994; Dadson et al., 2004; Lin et al., 2008; Hovius et al., 2011; Parker et al., 2011; Huang and Fan, 2013; Li et al., 2014, 2017). Thousands of landslides can be triggered by the seismic shaking. These coseismic landslides generate large amounts of debris, part of which will reach large streams and form landslide-dammed lakes that impound large volumes of water and sediments (Wang et al., 2011; Fan et al., 2012, 2017b; Tang et al., 2018). More debris will deposit, with marginal stability, high on the slopes and in low-order channels (Meunier et al., 2008; Gorum et al., 2011; Kargel et al., 2016; Fan et

30 al., 2018a, 2018b). It will be remobilised easily by minor storms (Dadson et al., 2004; Lin et al., 2006, 2008; Okamoto et al.,

2012; Huang and Fan, 2013; Fan et al., 2018b) and generate large flow-like landslides (Xu et al., 2012; Liu et al., 2014; Hu et al. 2017, 2018a, 2018b, 2018c). The earthquake-induced enhanced weakening and weathering of rock and soil masses will also cause delayed slope failures and sustain high erosion rates for a long time (Koi et al., 2008; Okamoto et al., 2012; Parker et al., 2015; Fan et al., 2017a, 2018d; Massey et al., 2018; Scaringi et al., 2018). These processes are a major source of hazard

5   to the population and the infrastructure. Earthquake-triggered chains of geohazards are major contributors to the tolls of damage and fatalities and to the costs for reconstruction and recovery of the socioeconomic fabric after large earthquakes (Huang and Fan, 2013; Wang et al., 2014; Cerè et al., 2017).

Observations on the evolution of mass wasting after recent major earthquakes reveal a peak of landslide rates (remobilisations of coseismic landslide deposits and post-seismic landslides) soon after the earthquakes, followed by decay

10   and normalisation within less than a decade (Fan et al., 2018a; Hovius et al., 2011; Marc et al., 2015; Zhang et al., 2016; Zhang and Zhang, 2017). The reasons for this normalisation, which seems quicker than that of the sediment export by non-landslide processes (Ding et al., 2014; Wang et al., 2015, 2017), are still poorly understood. Various processes, such as the progressive depletion of the debris, grain coarsening and densification, restoration of the vegetation cover and bedrock healing have been shown to play a role (e.g., Shieh et al., 2009; Zhang et al., 2014; Hu et al., 2018c; Marc et al., 2018; Yang et al., 2018). Analyses

15   of complete inventories that track the decay of landslide rates, together with laboratory and field-scale investigations and physically-based models, can certainly provide further insights.

1.2 Multi-temporal inventorying of landslides

Landslide mapping and inventorying at various scales are fundamental tools to investigate the spatial patterns of mass movements, track their evolution and reveal topographic, seismic, geological, hydrological, climatic, biological and

20   anthropogenic preconditions and controls to their distribution and fate (e.g., Guzzetti et al., 2002, 2009, 2012; Galli et al., 2008; Harp et al., 2011; Parker et al., 2015; Gariano and Guzzetti, 2016; Broeckx et al., 2018). Coseismic landslide inventories are compiled after major events with increasing quality and completeness (Keefer, 2002; Schmitt et al., 2017; Tanyas et al., 2017). They are fundamental for assessing the extent of the earthquake-affected areas and drive the post-earthquake emergency response, and can also provide information on the earthquake mechanisms (Gorum et al., 2011; Fan et al., 2018c). Besides,

25   complete and detailed inventories are necessary to evaluate the landscape response to earthquakes quantitatively, and to calibrate descriptive and predictive models effectively (Xu et al., 2014; Marc and Hovius, 2015; Marc et al., 2016a, 2016b, 2017). Several coseismic landslide inventories have been released and some of them have been collected into a common repository (Schmitt et al., 2017). This will promote standardisation of data collection and presentation and will facilitate meta-analyses and modelling efforts greatly.

30   Landslide inventories that cover several temporal scenes before and after major earthquakes are much less common. The interest around the temporal evolution of landsliding after major earthquakes has increased greatly in the past decades, particularly after the 1999 M_w 7.7 Chi-Chi earthquake and the 2008 M_w 7.9 Wenchuan earthquake (Dadson et al., 2004; Fan et al., 2018a, 2018b; Lin et al., 2008; Saba et al., 2010; Hovius et al., 2011; Marc et al., 2015; Tang et al., 2016; Yang et al.,

2016, 2018; Zhang et al., 2016; Zhang and Zhang, 2017). Research has been facilitated by the increased availability of frequent and high-resolution remote sensing images (Fan et al., 2018b), and by near real-time monitoring networks (Huang et al., 2015). However, to our knowledge, none of the multi-temporal inventories of post-seismic landslides compiled so far have been released to open repositories. With this paper and the related datasets, we wish to share our mapping work and monitoring data

5   to facilitate further analyses and meta-analyses by the research community. We also wish to encourage other researchers to share their data, with the aim of building a collection of datasets that will help advance the knowledge in the field.

2 Study area

Our datasets cover portions of the region affected by the M_w 7.9 Wenchuan earthquake at various levels of detail (Figure 1). The earthquake hit the Longmen mountains (Longmenshan) in west Sichuan, China, at the eastern margin of the Tibetan

10 plateau on May 12th, 2008, with a fault rupture that propagated from the epicentre along the range for about 240 km (Gorum et al., 2011; Huang and Fan, 2013; Fan et al, 2018b). Details on the tectonic setting of the Longmenshan and on the Wenchuan earthquake mechanisms, as well as geological and geomorphological characterisations of the region, can be found in several earlier works (Chigira et al., 2010; Qi et al., 2010; Dai et al., 2011; Gorum et al., 2011) to which the reader is referred for further information.

15 According to a recent inventory (Xu et al., 2014), the Wenchuan earthquake triggered almost 200,000 coseismic landslides over an area larger than 110,000 km². The total landslide area was estimated in about 1,160 km² (Xu et al., 2014), and the total landslide volume in the order of several km³ (Parker et al., 2011; Li et al., 2014; Marc and Hovius, 2015; Xu et al., 2014, 2016). Rain-induced post-seismic failures of deposits of coseismic debris, often evolving into catastrophic debris flows and floods, have been occurring frequently since after the earthquake (Tang et al., 2009, 2011, 2012; Xu et al., 2012; Guo et al.,

20 2016, 2017).
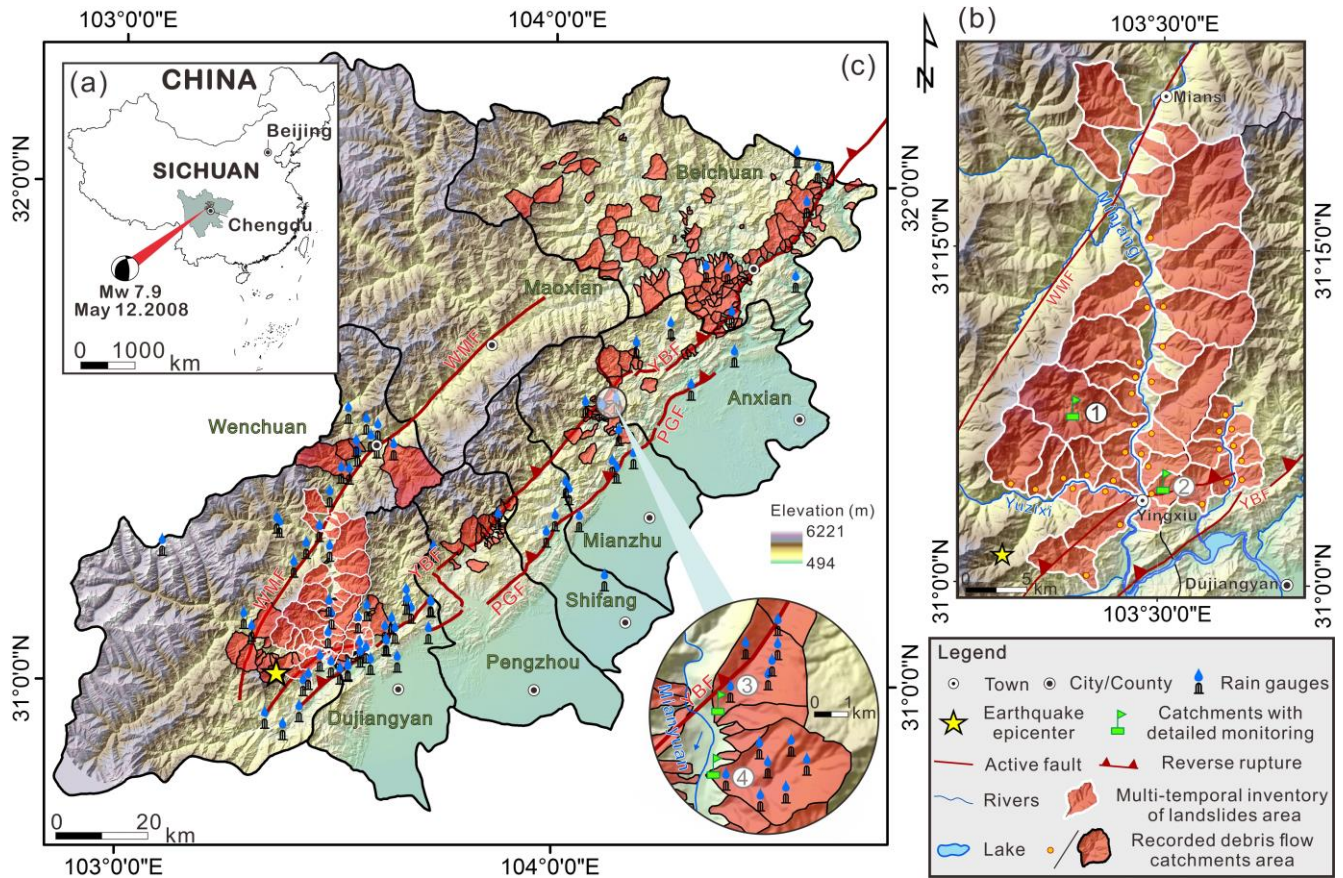
Figure 1. General view of the study area in Sichuan, China (a); Detail of the area in which the multi-temporal inventory of landslides was carried out (b); Detail of the area in which debris flows were recorded, with indication of their location and those of the rain gauges (c). Circled numbers (1-4) indicate well-monitored catchments.

2.1 Inventory of landslides

Our multi-temporal inventory of pre- and coseismic landslides, post-seismic remobilisations and new failures covers a significant portion of the earthquake's epicentral area. It is the largest area affected by the Wenchuan earthquake that has been covered by a detailed multi-temporal landslide inventory thus far (Fan et al., 2018a). The area comprises 42 catchments over 462.5 km^2 from the town of Yingxiu (the epicentre) to the town of Wenchuan (Figure 1b). It has been affected by coseismic landslides with a total volume of 0.8-1.5 billion m^3, according to empirical area-volume scaling relationships (Parker et al., 2011; Xu et al., 2016).

The region has rugged mountains with elevations that climb rapidly from 420 m a.s.l. in the main river valley to over 4,000 m a.s.l. on the mountain ridges. The slopes are generally steep, with more than half of them being steeper than 36°. Two of the main faults of the Longmenshan, the Wenchuan-Maowen and the Yingxiu-Beichuan faults (e.g., Qi et al., 2010), delimit this study area. Beneath a dense vegetation and a variably-thick soil cover lie weathered and highly fractured rocks, mostly igneous

(granite, diorite), though metamorphic and sedimentary rocks (schist, shale, sandstone, limestone) are also present, as well as recent Quaternary deposits. The climate is subtropical, affected by the monsoonal circulation, with 13 ºC of mean annual temperature and >1,250 mm/year of precipitation that mostly occurs in the summer months. The Min river (Minjiang), a tributary of the Yangtze river in its upper course, crosses the region through Wenchuan and Yingxiu and discharges, in average,
5   452 m^3/s of water (Tang et al., 2011).

2.2 Inventory of debris flows and triggering rainfalls

The dataset of debris flows and their triggering rainfalls covers 16,959 km^2, from the epicentre (near the town of Yingxiu) to the edge of the thrust-dominated portion of the seismogenic fault rupture (near the town of Beichuan). In this region, 527 debris flows affecting 244 catchments were identified. These catchments cover altogether about 1,581 km^2 (Figure 1c), and
10   spread along 177 km out of the 246 km of the fault surface rupture.

The study area is mountainous with elevations from 420 m a.s.l. in the river valley to almost 6,100 m a.s.l. on the ridges of the Hengduan mountains. A general northeast to southwest orientation is shown by the geological structures and the strike of the rock strata, and the bedrock outcrops are highly fractured and weathered. Most of the low-order channels are deeply cut and the slopes are steep, with a morphology that is strongly controlled by the high tectonic activity (Guo et al., 2016). The
15   climate is generally monsoon-influenced, with precipitations concentrated in the summer months. However large variability exists within the region, with the central and southern parts receiving annual precipitations exceeding 1,200 mm and easily reaching 2,000 mm, and the western part being drier and receiving less than 800 mm/year of precipitation (Guo et al., 2016).

The complex geology and the patterns of precipitation (with frequent rainstorms delivering hundreds of mm of rain in single events) make the area highly prone to debris flows. In the decades preceding the Wenchuan earthquake, some 250 debris
20   flows were recorded (Cui et al., 2008), and hundreds more were triggered after the earthquake which affected more than 800 streams within the first two years (Cui et al., 2011). The characteristics of the rain events that triggered debris flows changed abruptly upon the earthquake, displaying significantly lowered critical rainfall intensity and duration, and a pattern of gradual recovery over a decadal time scale (e.g., Yu et al., 2014; Guo et al., 2016, 2017).

3 Data and methods

25   Here we provide details of the source data and the preparation of our inventories. We also include some figures and tables that illustrate the contents of the inventories and some simple analyses.

3.1 Multi-temporal inventory of landslides

3.1.1 Imagery, mapping technique, attributes

We compiled the inventory through visual interpretation (following Harp et al., 2011) of high-resolution aerial and satellite
30   images (Spot 5, Spot 6, Worldview 2, Pleiades). In total, six sets of images were acquired, covering the period from 2005 to

2015 (Table 1). We selected these scenes according to the date of acquisition, coverage, absence of clouds and resolution. The areal coverage of the images is close to 99% in 2007, 2011 and 2015, 97% in 2008, 95% in 2013, and 93% in 2005. The 2011 scene was used as the geo-referencing base in ArcGIS environment (Environmental Systems Research Institute, Inc., United States) and the orthorectification was performed using the software Pix4D (Pix4D S.A., Switzerland). A 25-m resolution digital

5 elevation model, obtained from the Sichuan Bureau of Surveying and Mapping, was used to delineate the catchment boundaries.

Our inventory (Figures 2-3) provides a polygon-based delineation of landslides that occurred before the earthquake (2005 and 2007 scenes), which can be used to define the pre-earthquake landslide rates and patterns in studies focusing on a short-term time window. The 2008 scene was used to delineate the coseismic landslides; the 2011, 2013 and 2015 scenes were used

10 to identify the new landslides that occurred after the earthquake (i.e. the post-seismic landslides) and the remobilisations of coseismic landslides (i.e., the post-seismic remobilisations).

The landslide areas were differentiated into three types: slides, debris flows and channel deposits. Slides were mapped as such if preferential movement paths could not be identified in their debris-covered deposition areas. This type comprises debris and rock slides and debris and rock falls (see Hungr et al., 2014, for definitions of the landslide types). This simplification

15 derives from a lack of discernibility, in the remote sensing images, between these types of movement and their combinations. Differently, debris flows exhibited a finer material texture along a preferential movement path. They were found along the hillslopes and into small channels. Large amounts of accumulated debris were also found in main channels and were mapped as channel deposits. Some examples of landslide types are given in Figure 4.

To facilitate the visualisation and comparison of some results (see Figure 3 and Figure 5), we defined four levels of activity

20 to classify the landslide remobilisations, following Tang et al. (2016). A level of activity A1 was assigned if less than 1/3 of the coseismic or post-seismic landslide area displayed signs of remobilisation; a level A2 was assigned if the remobilisation involved between 1/3 and 2/3 of the area; a level A3 was assigned if the remobilisation involved more than 2/3 of the area. Finally, a level A0 was assigned if no remobilisations were identified (i.e. the landslide was dormant or its movement was too slow to produce changes that could be seen from the available imagery).

Table 1. Reference images used to map the landslides, acquisition date and attributes of each layer contained in the dataset. An additional shape file is provided to define the catchment boundaries and have a simple characterisation (CID: catchment identifier, catchment name and county, gradient and internal relief, drainage density and channel length).

Name of the layer (.shp)	Reference image: source / resolution / band	Acquisition date	Attributes
DF_Catchments		-	Shape, Name, CID, Country, Area, Grad_chan, Grad_Mchan, Grad_catch, Leng_chan, Drain_Dens, Reli_Mchan, Reli_chan, Reli_catch
2005	Spot 5 / 2.5 m / multispectral	Pre-earthquake (July 2005)	ID, Shape, Area, CID
2007	Landsat 4 / 30 m / multispectral	Pre-earthquake (September 2007)	ID, Shape, Area, CID
2008	Aerial photos / 1-2.5 m / RGB-panchromatic	Coseismic (May-July 2008)	ID, Shape, Area, Type, CID
2011	Aerial photos + Worldview 2 / 0.5-1 m / RGB-pansharpened	Post-seismic (April 2011)	ID, Shape, Area, Type, Act_level, CID
2013	Aerial photos + Pleiades / 0.5-2 m / RGB-panchromatic + multispectral	Post-seismic (April 2013)	ID, Shape, Area, Type, Act_level, CID
2015	Spot 6 / 1.5 m / pansharpened	Post-seismic (April 2015)	ID, Shape, Area, Type, Act_level, CID

Attributes: Shape (type of element: polygon, line, point); Name (Name of each catchment); CID (identifier for each catchment); Country (Name of the country where the catchment is located); Area (Area of each element in m^2); Grad_chan (mean slope of the whole channels present in the catchment in decimal degrees); Grad_Mchan (mean slope of the main channel present in the catchment in decimal degrees); Grad_catch (mean slope of the catchment in decimal degrees); Leng_chan (total length of the channels present in the catchment in m); Drain_Dens (Leng_chan/Area in m^{-1}); Reli_Mchan (Relieve of the main channel: highest altitude minus lowest altitude of the main channel in m), Reli_chan (Relieve of all the channels present in the catchment: highest altitude minus lowest altitude of the channels m), Reli_catch (Relieve of the catchment: highest altitude minus lowest altitude of the catchment m); ID (identifier of each element); Type (type of landslide: s – slide; d – debris flow; cd – channel deposit); Act_level (level of activity of the landslide: 0 – activity level A0, dormant landslide; 1 – activity level A1; 2 – activity level A2; 3 – activity level A3; 4 – new landslide).
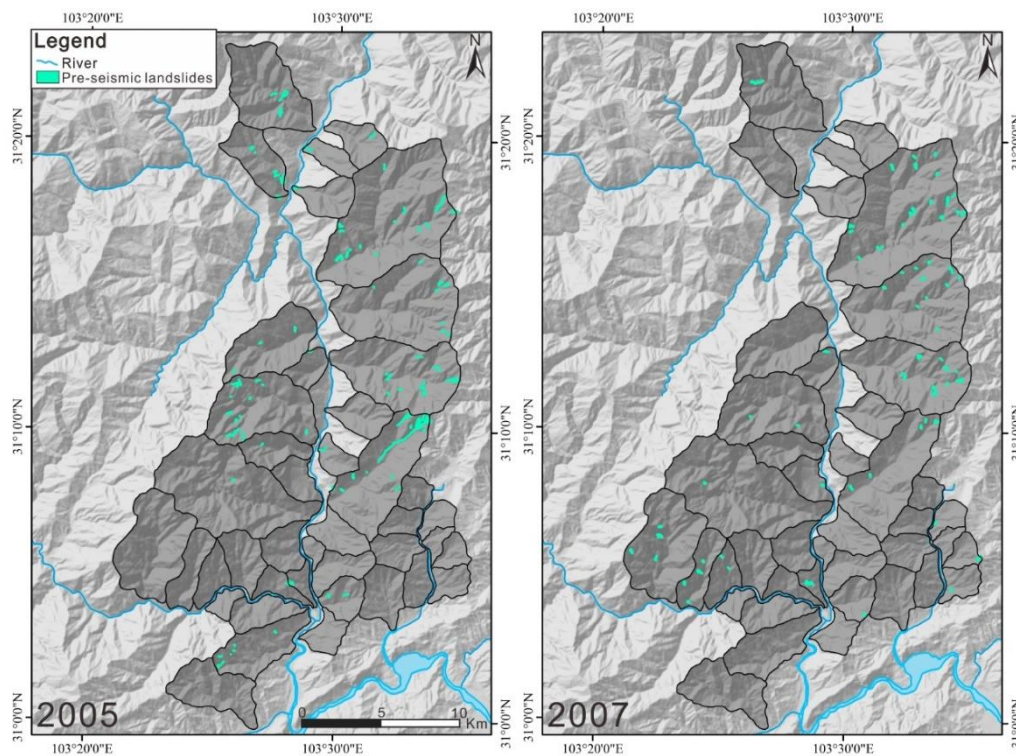
Figure 2. Landslides mapped from the 2005 and 2007 images (pre-earthquake).
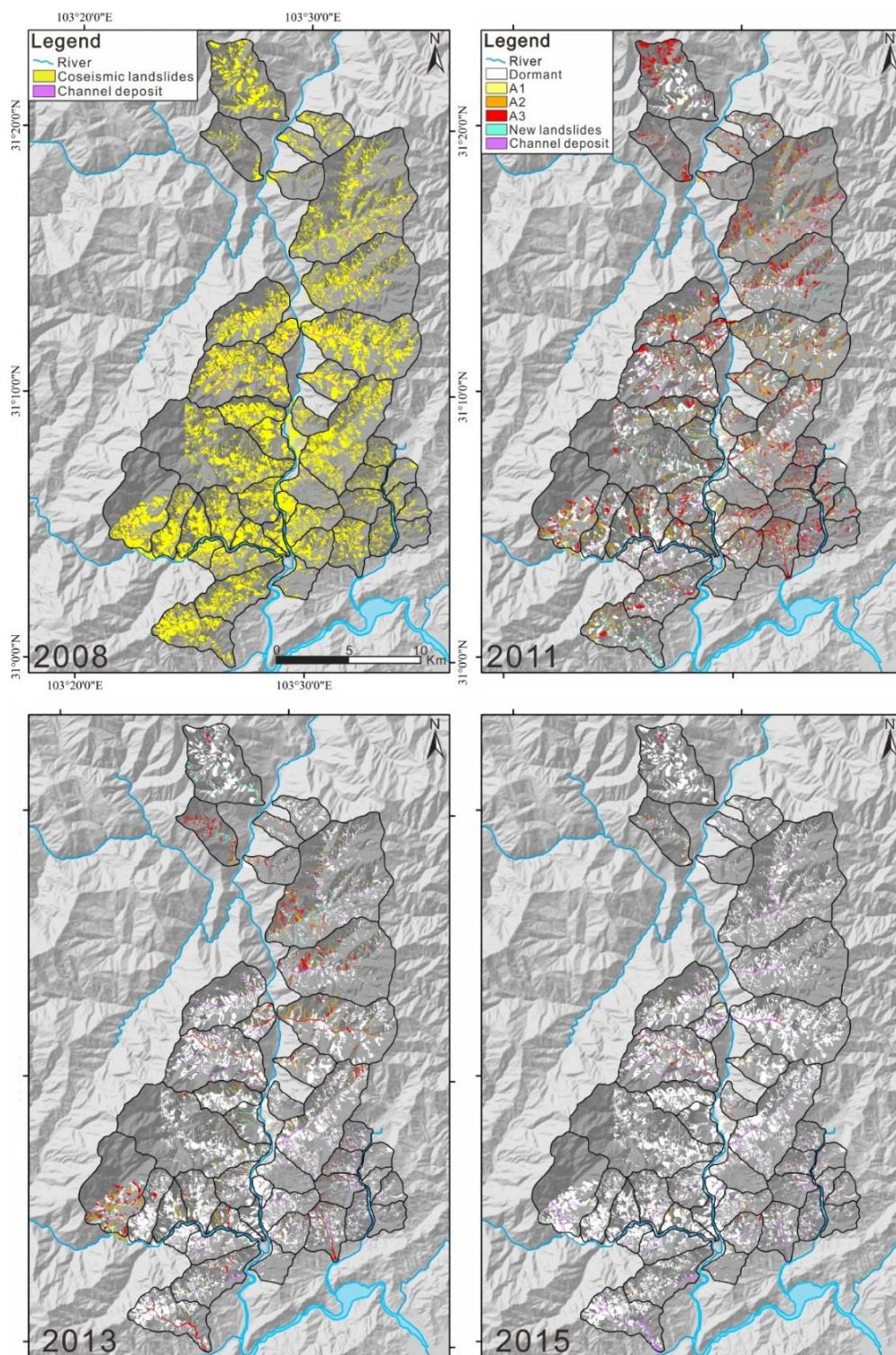
Figure 3. Coseismic and post-seismic landslides (years 2008, 2011, 2013 and 2015) with indication of the levels of activity.
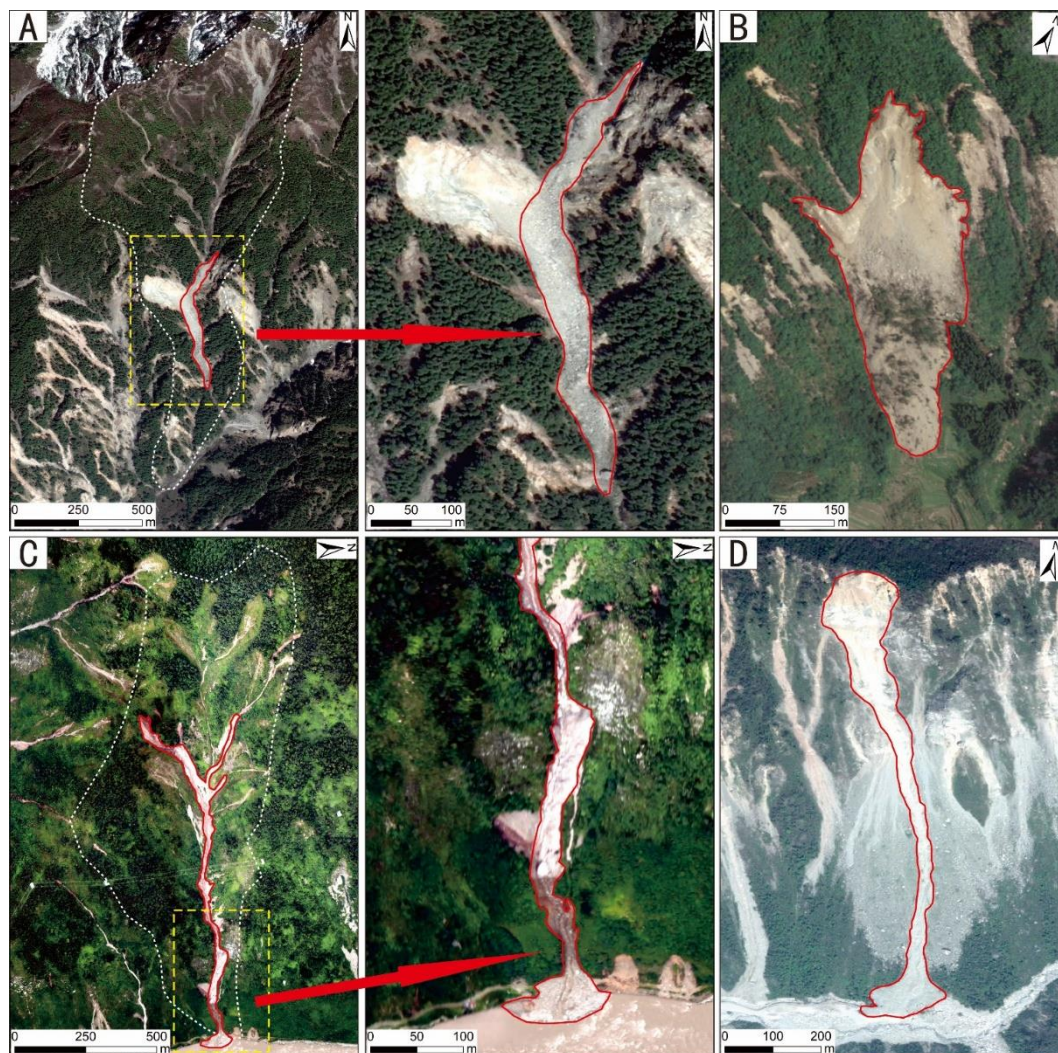
Figure 4. Types of landslides and deposits mapped in the inventory: channel deposit (A); slide (B), debris flow in a channel (C), debris flow on a hillslope (D).
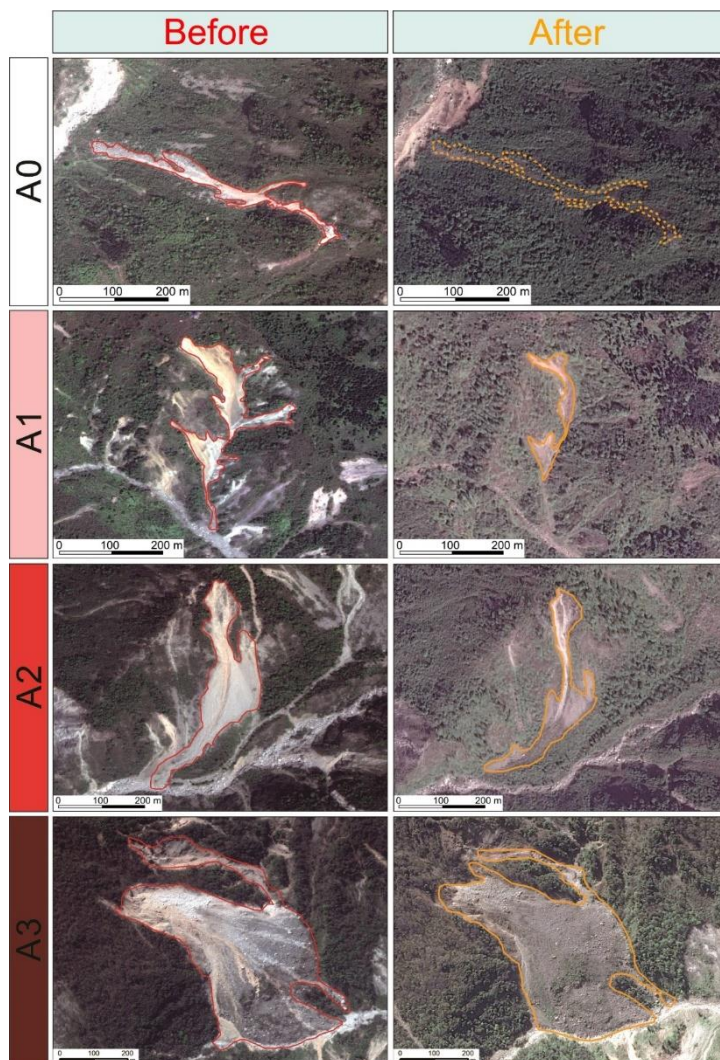
Figure 5. Examples of coseismic landslide deposits displaying different levels of activity.

3.1.2 Uncertainties

The processes of manual mapping and interpreting landslide boundaries and types are affected by unavoidable
5 uncertainties due to stochastic errors, variable quality of the remote sensing images, and variable experience of the mappers.
On the other hand, semi-automatic and automatic methods of landslide identification do not necessarily offer better
performances, and can even lead to larger uncertainties when applied to very high resolution images (van Westen et al., 2006;
Guzzetti et al., 2012; Pawłuszek et al., 2017). Moreover, some semi-automatic techniques still need visual interpretation over
a significant test area for calibration (e.g., Đurić et al., 2017), and automatic methods may require a combination of images of
10 different portions of the spectrum, or of satellite and aerial images, that should be acquired within a narrow time window to be

significant for a multi-temporal inventorying of fast evolving features. Such techniques are not necessarily less time consuming than the manual interpretation (Santangelo et al., 2015).

Our mapping was carried out by five mappers who worked on distinct areas with the same set of pre-agreed rules for the identification of the landslides and their types (see also Fan et al., 2018a). The mappers worked in close contact, interacting and discussing non-easily discernible cases. Nonetheless, we evaluated the individual performances of the mappers to make an estimation of the mapping uncertainties and their propagation into further analyses. We selected a test area (a portion of a catchment), on which accurate mapping had been performed for one scene (2011), which was verified and improved during field investigation. We assumed the landslide inventory for this test area to be good enough to consider the uncertainties negligible, and we used it as a reference. We asked each mapper to produce, independently, an inventory of the same area, which we compared to the reference inventory (Figure 6). We evaluated the matching degree between each mapper's inventory and the reference inventory, M_n, which we defined as follows:

$$M_n = \frac{A_n \cap A_r}{A_r}$$

where A_n is the landslide area delineated by the *n-th* mapper and A_r is the respective area of the reference inventory. We then calculated the average matching degree of the team as follows:

$$M = \frac{1}{N} \sum_{n=1}^{N} M_n$$

where N is the number of mappers in the team. A matching degree $0.67 \leq M \leq 0.86$ was evaluated in the test area. In average, the landslide areas matched with those of the reference inventory by 76%, and an average mapping uncertainty of $\pm 19\%$ in terms of total landslide area was calculated. If this same value of uncertainty is assumed for the entire study area, this will be a conservative estimate, as the uncertainties will tend to decrease with the landslide areas increasing, and the test area consisted mostly of small landslides. We believe that this uncertainty can be acceptable when performing regional scale analyses, as it can be demonstrated that it does not affect the patterns of frequency-size distributions or potential controlling factors significantly (Fan et al., 2018a).
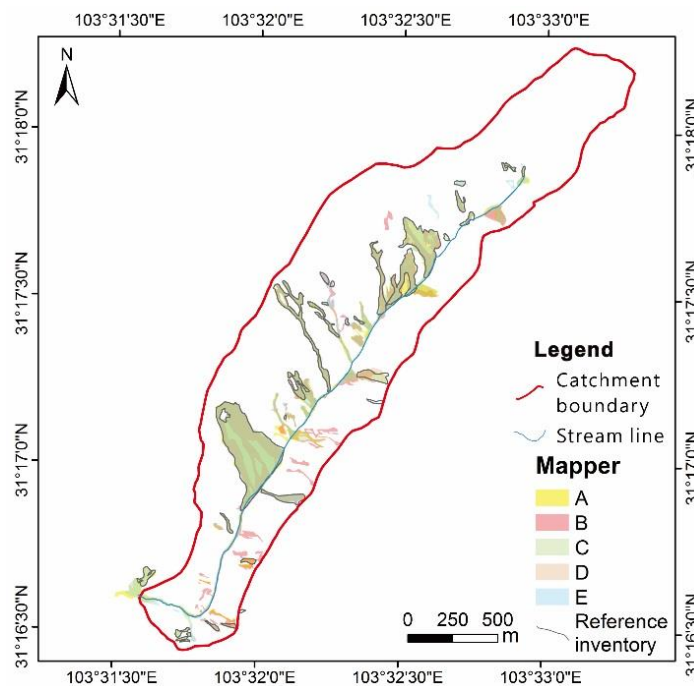
Figure 6. Landslide inventory of a test area (remote sensing image of 2011): comparison between the reference, field checked inventory with those produced by five mappers (A-E) independently, on the basis of the sole imagery and a common set of rules. Darker shades indicate areas in which most inventories overlap.

3.1.3 Simple statistics

We identified 133 and 71 pre-seismic landslides from the 2005 and 2007 scenes, respectively, and 8,917 coseismic landslides from the 2008 scenes, of which 8,259 were classified as slides, 571 as debris flows and 87 as channel deposits. We also delineated 832 new landslides from the 2011 scenes (589 slides, 193 debris flows, 50 channel deposits), 387 from the 2013 scenes (254 slides, 106 debris flows, 27 channel deposits), and 14 from the 2015 scenes (7 slides, 1 debris flow, 6 channel deposits). From the 2011, 2013 and 2015 scenes we identified 4099, 1152 and 273 landslides, respectively, with levels of activity A1-A3. More details are given in Table 2. Notice that these numbers are slightly different from those published by Fan et al. (2018a), although they referred to the same study area, because the inventory has been refined since then.

The number of coseismic deposits that were reactivated in each period, the area affected by the reactivation, the number and areas of first-failure landslides decreased significantly over time (Table 3). The coseismic landslides covered 124 km^2; only 37 km^2 had some activity (A1-A3) in 2011, while only 14 km^2 were active in 2013 and 6 km^2 in 2015. Furthermore, the degree of activity of the coseismic deposits rapidly decreased and, with time, the number and areas of active slides decayed faster than that of debris flows.

The frequency-size distribution analysis (e.g., Malamud et al., 2004) carried out with the dataset (Figure 7) show the patterns of pre- and coseismic landslides and post-seismic remobilisations for the period 2005-2015. The largest number of

landslides was triggered by the earthquake, while and the post-seismic rates of remobilisation decreased in the following years. This decrease mostly occurred for landslides with small areas, while the curves do not exhibit important changes in the range of landslides with large area ($A > 10^5$ m^2).

Table 2. Landslides with no information (NI), channel deposits (cd), slides (s), debris flows (d), levels of activity (A0-A3) and new landslides (NL) in the inventory.

Year	NI	cd	Activity level				NL	s	Activity level				NL	d	Activity level				NL
			A0	A1	A2	A3			A0	A1	A2	A3			A0	A1	A2	A3	
2005	133	-	-	-	-	-	-	-	-	-	-	-	-	-	-	-	-	-	-
2007	71	-	-	-	-	-	-	-	-	-	-	-	-	-	-	-	-	-	-
2008	-	87	-	-	-	-	-	8259	-	-	-	-	-	571	-	-	-	-	-
2011	-	122	12	9	11	40	50	7955	4406	860	739	1361	589	1676	404	306	332	441	193
2013	-	134	75	1	8	23	27	8799	7758	310	192	285	254	1096	657	132	107	94	106
2015	-	178	106	33	8	25	6	9016	8906	66	14	23	7	930	825	65	19	20	1

Table 3. Simple statistics of the landslides included in the multi-temporal inventory. Note that the volumes in this table were calculated according to the area-volume scaling proposed by Xu et al. (2016). A_{min}, A_{max}, $A_{average}$, A_{total} and V_{total} are, respectively, the minimum, maximum, average and total area of landslides, and their estimated total volume.

	A_{min} (m^2)	A_{max} (m^2)	$A_{average}$ (m^2)	A_{total} (m^2)	V_{total} (x10^6 m^3)
2005	156	54,550	5,412	719,817	15,749,964
2007	1995	38,770	14,423	1,024,062	24,116,037
2008	30	584,700	13,917	124,098,226	7,945,886,517
2011$_{remobilised}$	35	348,195	8,924	36,580,002	1,815,543,690
2011$_{new landslides}$	44	514,284	5,880	4,892,221	159,622,734
2013$_{remobilised}$	55	461,738	12,140	13,986,239	568,075,756
2013$_{new landslides}$	121	473,171	8,575	3,318,339	99,852,603
2015$_{remobilised}$	35	372,561	21,263	5,804,788	196,273,869
2015$_{new landslides}$	1,672	73,974	13,303	186,240	3,074,042
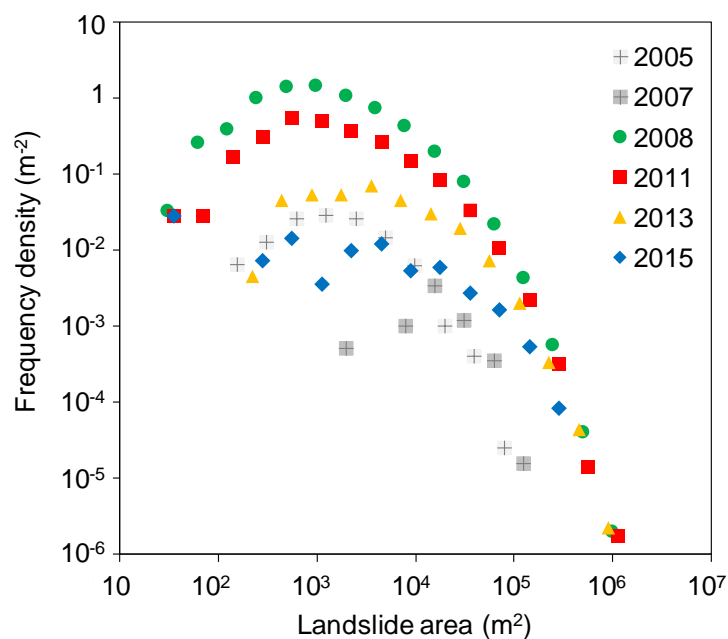
Figure 7. Frequency density – size distributions of pre-seismic landslides (2005-2007), coseismic landslides (2008) and post-seismic remobilisations (2011-2015) in the landslide inventory.

3.2 Inventory of debris flows and their triggering rainfalls

3.2.1 Data acquisition, structure of the dataset and attributes

We compiled a dataset of debris flows which occurred after the 2008 Wenchuan earthquake until the rainy season in summer 2017. These events are associated to the recordings of rain gauges and are spread over an area of 16,959 km^2.

The structure of the dataset is summarised in Table 4. The dataset contains information on the locations, date and time of occurrence of debris flows, and on the rainfalls that triggered them. We included data not only for catastrophic and well-studied events (e.g., Tang et al., 2012; Xu et al., 2012), but also for smaller events that did not cause fatalities or heavy damage to the population and the infrastructure. We used a 25-m resolution digital elevation model, provided by the Sichuan Bureau of Surveying and Mapping, to define the catchment boundaries. The rainfall data were obtained from the Meteorological Administration of China, from the Meteorological Bureau of Sichuan Province, from the bureau of land and resources of Chengdu and from the WebGIS monitoring network of the State Key Laboratory of Geohazard Prevention and Geoenvironment Protection (SKLGP, Chengdu, China; see Huang et al., 2015). These data were all recorded by automatic rain gauges.

We verified most of the debris flows included in the dataset through field investigation, literature review and interviews to the local residents. The debris flows were georeferenced through the latitude and longitude of the outlet of the catchment in

which they occurred. Information on the rainfall that triggered each debris flow is provided for the rain gauges located in closest proximity to them (< 5 km). In case no rain gauges were actively recording within this distance, data from the closest rain gauge are provided. We chose to provide rainfall data with the highest resolution available (in most cases hourly rainfall, in some cases 10-minutes rainfall) for a time window starting from one week before until one day after the debris flow event.

5   The choice of this window should allow for the inclusion of the significant antecedent rainfall in our setting, that can be used for further analyses of the triggering conditions of the debris flows. If the reader requires them, rainfall series with wider time windows can be obtained from the authors upon request.

For one catchment (Er catchment; No. 1 in Figure 1b; Table 5; Cui et al., 2018), we release data series of rainfall intensity, flow discharge, density and height. The Er catchment is administratively part of Yingxiu township and covers 39.4 km^2 with

10   a channel length of 11.5 km. The Ergou River flows within the catchment, which is a tributary of the Minjiang River. The headwater elevation of the catchments is 4,120 m a.s.l. and the outlet is located at 990 m a.s.l. Rainfall intensity was obtained through rain gauges with 0.5-mm tipping buckets. Flow discharge was calculated as the product of the cross-sectional mean velocity and the cross-sectional area of the flow. The latter was calculated from the depth, obtained from the data measured by the ultrasonic stage meter, in combination with the detailed geometry of each section. The surface velocity of the flow was

15   measured using automatic radar speed indicators and compared with video images. Flow depths were measured using ultrasonic stage meters TSS908, Beijing Guda instrument Co., Ltd.), with 1-min recording frequency, 0–30 m measurement range and ±10 mm error. For other well-monitored catchments (No. 2, 3 and 4 in Figure 1b), we release rainfall data for three important debris flow events (see Section 3.2.3, below), while full data series are available from the authors upon request.

Table 4. Structure of the dataset of debris flows and their triggering rainfalls. An additional shape file is provided to define the
20   **catchment boundaries with a simple characterisation (CID, catchment name and county, gradient and internal relief, drainage density and channel length).**

Folder name	File name	File type	Layers/sheets	Attributes (columns)
DF_RG_inventory	DF_RG_inventory	Shape file (.shp) and spreadsheet (.xls)	debris_flows	DF_ID, CID, Gully_name, Latitude, Longitude, Year, Month, Day, Time_24h_, T_Comment, Source_vol, Depo_vol, List_of_RG, Monitoring, Reference
			rain_gauges	RG_ID, CID, coordinates, temporal resolution, units, data references
R_DF_ID_X*	A_B_CDEF	Spreadsheet (.xls)	-	date and time, amount of rain

Attributes: DF_ID: identifier of the debris flow; CID: identifier of the catchment to which the debris flow or the rain gauge belong; Gully_name: name of the catchment; Latitude: latitude of the debris flow event (°); Longitude: longitude of the debris flow event (°); Year: year the debris flow event occurred; Month: month the debris flow event occurred; Day: day the debris flow event occurred; Time_24h_: time at which the debris flow occurred (24 h); T_Comment: specifications on the time of occurrence of the debris flow; Source_vol: available material during the initiation of the debris flow (m^3); Depo_vol: volume of debris flow deposited at the fan area (m^3); List_of_RG: list of rain gauges (identifier) located in proximity to the debris flow event that were actively recording throughout the time window of interest for that debris flow; Monitoring: specifies if additional monitoring data are available for that event (Y: yes; N: no); References: source of each debris flow event.
* one folder for each debris flow event being "X" the debris flow event identifier (DF_ID). Each folder contains the rain gauges located within a distance of 5 km for a given event. "A" indicates the relative position of each rain gauge from the debris flow event in

ascending order; "B" refers to the rain gauge identifier (RG_ID); C, D and E indicate the year, month and day of the debris flow event, respectively, and F refers to the starting time of the rain. Rain is expressed in mm. Each spreadsheet provides data from 7 days before to one day after the date associated with the debris flow event (DF_ID). Full data series are available, from the authors upon request, for further analysis.

Table 5. Released information on well-monitored catchments.

File name	File type	Sheets	Attributes (columns)
Er_vel_rain_disc_dens	Spreadsheet (.xls)	debris_flows	Latitude and Longitude of each station (°), Rainfall intensity measured at R1 (mm/h); Discharge measured at S1, S2 and S3 (m^3/s); Flow density measured at S1 (g/cm^3) and Flow depth (m) vs flow velocity (m/s) measured at S1 (Peng et al., 2018)
Rainfall distribution	Spreadsheet (.xls)	Qingping_a	Rain gauge coordinates, Date, Daily rainfall (mm), Cumulative rainfall (mm) (You et al., 2018)
		Qingping_b	Rain gauge coordinates, Date, Time (h), Hourly rainfall (mm), Cumulative rainfall (mm) (You et al., 2018).
		Hongchun	Rain gauge coordinates, Date, Time (h), Hourly rainfall (mm), Cumulative rainfall (mm) (Tang et al., 2011)
		Er	Rain gauge coordinates, Date, Time (h), Hourly rainfall (mm), Cumulative rainfall (mm) (Cui et al., 2018)

3.2.2 Uncertainties

Especially for minor debris flows, the time of debris flow occurrence may be uncertain, especially in those locations that lack proper instrumentation or eyewitnesses. Moreover, ambiguities in the definition of this time, as the debris flow has a finite duration, may occur. In this work, the time refers to the arrival of the flow at the outlet of the catchment, unless otherwise stated. In most cases, the debris flows in the study area were able to travel to the catchment outlets within 1 hour from their initiation (Guo et al., 2016), hence the time of debris flow initiation, if needed for analyses and modelling, can be estimated in this way.

Rainfall recordings from rain gauges located within or near a catchment in which a debris flow developed are not equally representative of the rainfall that actually triggered the debris flow and permitted its runout. In our dataset we decided to be inclusive by using a wide buffer around the event location, not to discard some data series that may be useful for analyses of rainfall variability at local scale and to perform interpolations. However, it is worth reminding that the spatio-temporal patterns of rainfalls in mountainous areas can be extremely inhomogeneous (e.g., Nikolopoulos et al., 2014). Significant variations may exist even within the same catchment, over distances of a few km or even just a few hundreds of metres (e.g., Smith et al., 2003; Panziera et al., 2011), in dependence, for instance, on the variability of the elevation, slope and aspect of the area, in

combination with the local pattern of wind at the time of the rain event. Moreover, rain gauges are usually installed in valleys and channels, while debris flows originate high on the slopes (Stoffel et al., 2011), which can generate a systematic bias. The uncertainties that derive from imperfect choices of the representative rain gauge(s) for a debris flow event have been shown to lead to large underestimations of the debris flow-triggering thresholds and to strongly limit the performance of warning systems

5 (Nikolopoulos et al., 2014; Guo et al., 2016, 2017). Therefore, these uncertainties should be carefully estimated and minimised with appropriate strategies whenever possible. Various studies, for instance, suggested the use of weather radar and satellite-based rainfall estimates to assess the representative rainfalls for debris flows (Kirschbaum et al., 2012; Rossi et al., 2012), but the literature featuring methods to address the issue of rainfall variability systematically is still poor (Jakob and Weatherly, 2003; Guzzetti et al., 2007; Jakob et al., 2012; Borga et al., 2014).

10 **3.2.3 Simple statistics**

The dataset contains information about 527 debris flows which occurred in 244 catchments, and rainfall data from 91 rain gauges. Most of the debris flows occurred during the summertime heavy rainfalls of 2008, 2010 and 2013, particularly in the counties of Wenchuan and Beichuan (Table 6).

In Figure 8, examples of rainfall data series are reported for well-monitored debris flow events in Qingping, Hongchun
15 and Er catchments (see Table 5). In Figures 9 and 10, the well-monitored debris flow event in Er catchment is shown (photographs, rainfall data, flow discharge, height and density).

Table 6. Simple statistics of the debris flows and their triggering rainfalls recorded in the dataset.

By year		By location		
Year	**No. of debris flows**	**Location**	**No. of debris flows**	**No. of catchments**
2008	195	Wenchuan	167	67
2009	25			
2010	167	Pengzhou	43	23
2011	36	Mianzhu	92	26
2012	29	Anxian	40	11
2013	68	Beichuan	185	117
2014	3			
2015	1			
2016	2			
2017	1			
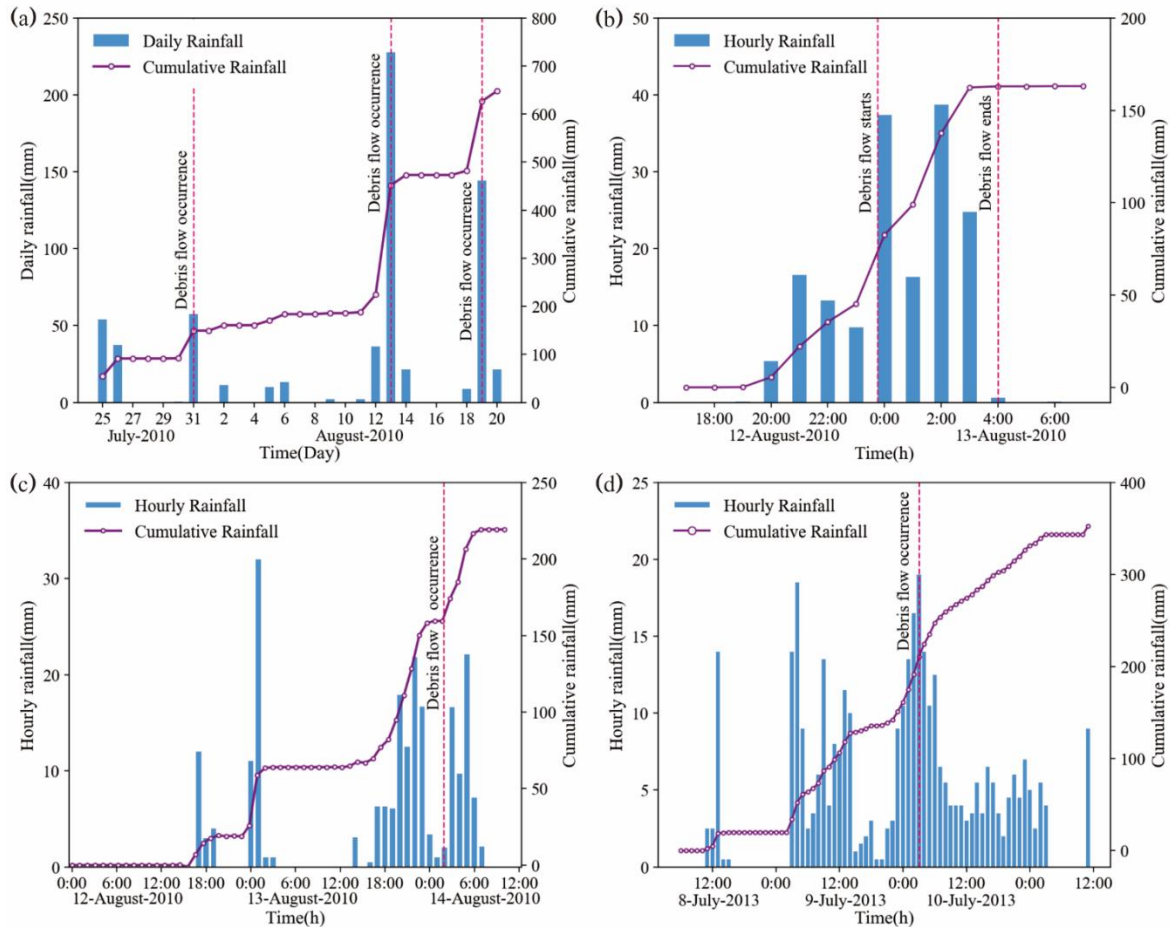
Figure 8. (a) Daily and accumulated precipitation in Qingping (Wenjia gully, CID M9, Mianzhu Country; No. 4 in Figure 1c) during a period affected by the three debris flow events. The DF_ID of these events are, chronologically, 272, 302 and 273. Rainfall data were recorded by a rain gauge located in Nanmu (CID M22, LAT 104.154533, LONG 31.48832, Yu et al., 2010). (b) Detail of the second debris flow (DF_ID 302) occurred between 12 and 13 August 2010 in Qingping: hourly and accumulated precipitations and event start and end are represented. (c) Hourly and accumulated precipitation in Hongchun (CID W25, Wenchuan country; No. 2 in Figure 1c). A debris flow occurred on 14 August 2010 (DF_ID 53). Rainfall data were recorded by a rainfall gauge located in Yingxiu (LAT 103.4826; LONG 31.06417). (d) Hourly and accumulated precipitation in Er (CID W7, Wenchuan Country; No. 1 in Figure 1c). A debris flow occurred on 10 July 2013 (DF_ID 164). Rainfall data were recorded by a rainfall gauge located in Er (LAT 103.46088; LONG 31.11679; R1 in Figure 10a; Cui et al., 2018).

Figure 9. Debris flow event recorded in Er (CID W7, Wenchuan Country; No. 1 in Figure 1c) on 5 July 2016 (Cui et al., 2018).
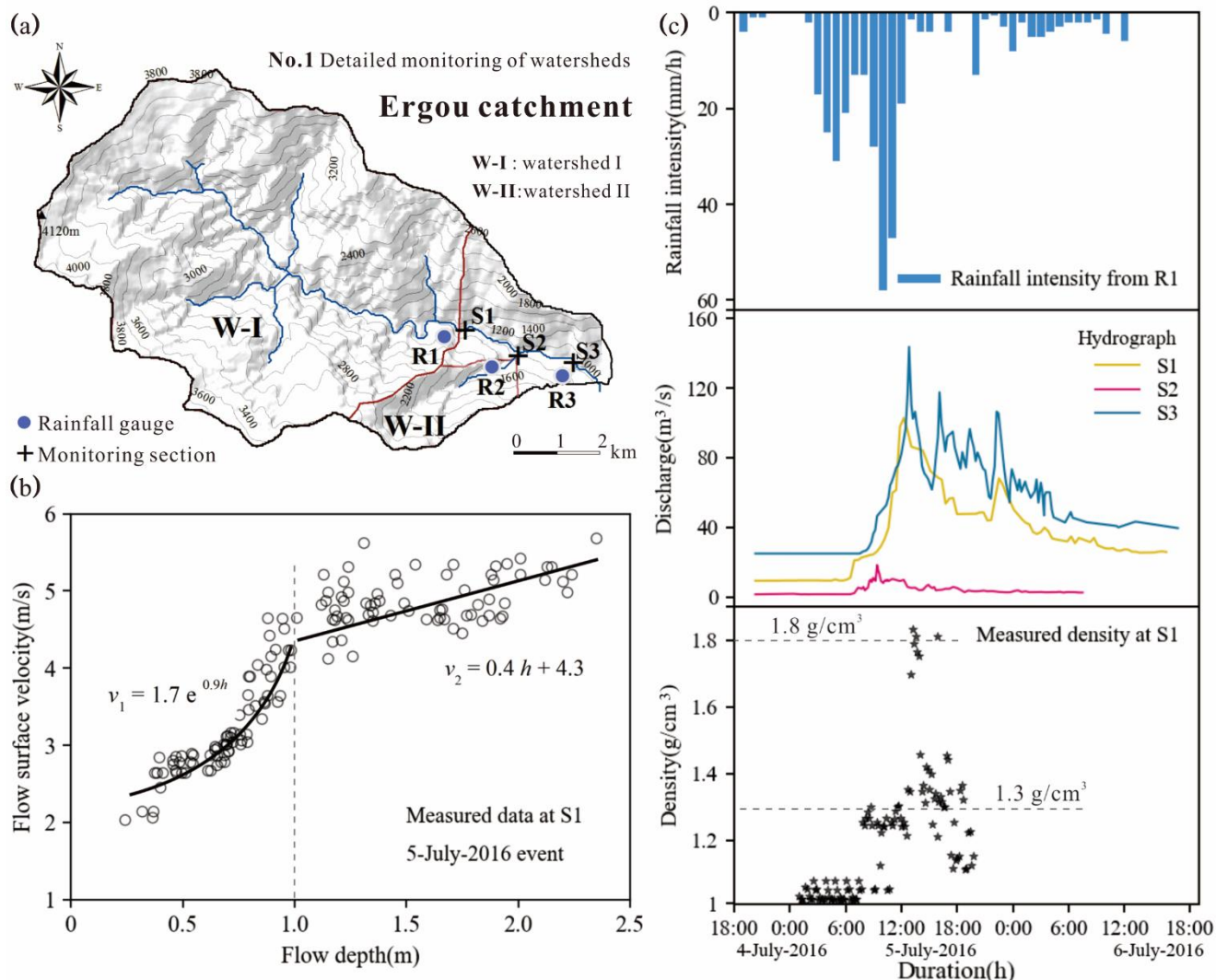
Figure 10. Data analysis of the debris flow which occurred on 5 July 2016 (Figure 9) in Er (CID W7, Wenchuan Country; No. 1 in Figure 1c; Cui et al., 2018). (a) Map of the catchment; (b) Flow surface velocity vs flow depth; (c) rainfall intensity, flow discharge and flow density.

4 Data availability

The datasets are freely available at https://doi.org/10.5281/zenodo.1405490 (Domènech et al., 2018). In addition to the data, the repository contains supplementary material (metadata files) that clarify the structures of the datasets, and a reference list for the data sources.

5 Summary

We presented a multi-temporal inventory of landslides in a portion of the area affected by the 2008 Wenchuan earthquake covering the period from 2005 to 2015 and an inventory of debris flows and their triggering rainfalls over a larger area covering the period from 2008 to 2017. The two datasets, which are freely available, can provide an insight into the spatial and temporal patterns of the enhanced mass wasting caused by a strong earthquake. We encourage other researchers to follow our example by sharing analogous datasets, to build an open collection of data and facilitate meta-analyses among multi-temporal datasets of mass wasting induced by earthquakes or other triggers.

6 Author contributions

XF designed the work, with frequent inputs from GD and GS; GS wrote the manuscript; GD, LD and FY compiled the datasets and prepared the display items; GD, LD, and FY performed the mapping supervised by XF; XG and CH provided some of the data, and suggestions on some methods; XF, RH and QX acquired project funds and supervised the project; all authors revised and approved the datasets and the manuscript.

7 Competing interests

The authors declare that they have no competing interests.

8 Acknowledgements

The collection and processing of the data presented in this paper were funded by National Science Fund for Excellent Young Scholars of China (Grant No. 41622206), the Funds for Creative Research Groups of China (Grant No. 41521002), the Fund for International Cooperation (NSFC-RCUK_NERC), Resilience to Earthquake-induced landslide risk in China (grant No. 41661134010). We also want to thank the contribution of all the group of experts during the mapping.

References

Borga, M., Stoffel, M., Marchi, L., Marra, F., and Jakob, M.: Hydrogeomorphic response to extreme rainfall in headwater systems: flash floods and debris flows, J. Hydrol., 518, 194-205, doi: 10.1016/j.jhydrol.2014.05.022, 2014.

Broeckx, J., Vanmaercke, M., Duchateau, R., and Poesen, J.: A data-based landslide susceptibility map of Africa, Earth Sci. Rev., 185, 102-121, doi: 10.1016/j.earscirev.2018.05.002, 2018.

Cerè, G., Zhao, W., Rezgui, Y., Parker, R., Hales, T., MacGillivray, B. H., and Gong, Y.: Multi-objective consideration of earthquake resilience in the built environment: The case of Wenchuan earthquake, 2017 International Conference on Engineering, Technology and Innovation (ICE/ITMC), Madeira Island, Portugal, pp. 513-520, 2017.

Chigira, M., Wu, X., Inokuchi, T., and Wang, G.: Landslides induced by the 2008 Wenchuan earthquake, Sichuan, China, Geomorphology, 118, 225-238, doi: 10.1016/j.geomorph.2010.01.003, 2010.

Cui, P., Wei, F. Q., He, S. M., You, Y., Chen, X. Q., Li, Z. L., and Yang, C.L.: Mountain disasters induced by the earthquake of May 12 in Wenchuan and the disasters mitigation. J. Mt. Sci., 26 (3), 280–282, 2008.

Cui, P., Chen, X. Q., Zhu, Y. Y., Su, F. H., Wei, F. Q., Han, Y. S., Liu, H. J., and Zhuang, J. Q.: The Wenchuan Earthquake (May 12, 2008), Sichuan Province, China, and resulting geohazards. Nat. Hazards, 56 (1), 19–36, doi: 10.1007/s11069-009-9392-1, 2011.

Cui, P., Guo, X., Yan, Y., Li, Y., and Ge, Y.: Real-time observation of an active debris flow watershed in the Wenchuan Earthquake area, doi: 10.1016/j.geomorph.2018.08.024, 2018.

Dadson, S. J., Hovius, N., Chen, H., Dade, W. B., Lin, J. C., Hsu, M. L., Lin, C. W., Horng, M. J., Chen, T. C., Milliman, J., and Stark, C. P.: Earthquake-triggered increase in sediment delivery from an active mountain belt, Geology, 32 (8), 733-736, doi: 10.1130/G20639.1, 2004.

Dai, F. C., Xu, X., Yao, X., Xu, L., Tu, X. B., and Gong, Q. M.: Spatial distribution of landslides triggered by the 2008 Ms 8.0 Wenchuan earthquake, China, J. Asian. Earth Sci., 40, 883-895, doi: 10.1016/j.jseaes.2010.04.010, 2011.

Ding, H., Li, Y., Ni, S., Ma, G., Shi, Z., Zhao, G., Yan, L., and Yan, Z.: Increased sediment discharge driven by heavy rainfall after Wenchuan earthquake: A case study in the upper reaches of the Min River, Sichuan, China, Quatern. Int., 333, 122-129, doi: 10.1016/j.quaint.2014.01.019, 2014.

Domènech, G., Yang, F., Guo, X., Fan, X., Scaringi, G., Dai, L., He, C., Xu, Q., Huang, R.: Two multi-temporal datasets to track the enhanced landsliding after the 2008 Wenchuan earthquake, version 1, Zenodo repository, doi: 10.5281/zenodo.1405490, 2018.

Đurić, D., Mladenović, A., Pešić-Georgiadis, M., Marianović, M., and Abolmasov, B.: Using multiresolution and multitemporal satellite data for post-disaster landslide inventory in the Republic of Serbia, Landslides, 14, 1467-1482, doi: 10.1007/s10346-017-0847-2, 2017.

Fan, X., van Westen, C. J., Korup, O., Görüm, T., Xu, Q., Dai, F., Huang, R., and Wang, G.: Transient water and sediment storage of the decaying landslide dams induced by the 2008 Wenchuan earthquake, China, Geomorphology, 171–172, 58-68, doi: 10.1016/j.geomorph.2012.05.003, 2012.

Fan, X., Xu, Q., Scaringi, G., et al.: Failure mechanism and kinematics of the deadly June 24th 2017 Xinmo landslide, Maoxian, Sichuan, China, Landslides, 14 (6), 2129-2146, doi: 10.1007/s10346-017-0907-7, 2017a.

Fan, X., Xu, Q., van Westen, C. J., Huang, R., and Tang, R.: Characteristics and classification of landslide dams associated with the 2008 Wenchuan earthquake, Geoenvironmental Disasters, 4, 12, doi: 10.1186/s40677-017-0079-8, 2017b.

Fan, X., Domènech, G., Scaringi, G., Huang, R., Xu, Q., Hales, T. C., Dai, L., Yang, Q., and Francis, O.: Spatio-temporal evolution of mass wasting after the 2008 Mw 7.9 Wenchuan Earthquake revealed by a detailed multi-temporal inventory, Landslides, doi: 10.1007/s10346-018-1054-5, 2018a.

Fan, X., Juang, C. H., Wasowski, J., Huang, R., Xu, Q., Scaringi, G., van Westen, C. J., and Havenith, H. B.: What we have learned from the 2008 Wenchuan Earthquake and its aftermath: A decade of research and challenges, Eng. Geol., 241, 25-32, doi: 10.1016/j.enggeo.2018.05.004, 2018b.

Fan, X., Scaringi, G., Xu, Q., Zhan, W., Dai, L., Li, Y., Pei, X., Yang, Q., and Huang, R.: Coseismic landslides triggered by the 8th August 2017 Ms 7.0 Jiuzhaigou earthquake (Sichuan, China): factors controlling their spatial distribution and implications for the seismogenic blind fault identification, Landslides, 15 (5), 967-983, doi: 10.1007/s10346-018-0960-x, 2018c

Fan, X., Xu, Q., and Scaringi, G.: Brief communication: Post-seismic landslides, the tough lesson of a catastrophe, Nat. Hazards Earth Syst. Sci, 18 (1), 393-403, doi: 10.5194/nhess-18-397-2018, 2018d.

Galli, M., Ardizzone, F., Cardinali, M., Guzzetti, F., and Reichenbach, P.: Comparing landslide inventory maps, Geomorphology, 94 (3-4), 268-289, doi: 10.1016/j.geomorph.2006.09.023, 2008.

Gariano, S. L., and Guzzetti, F.: Landslides in a changing climate, Earth Sci. Rev., 162, 227-252, doi: 10.1016/j.earscirev.2016.08.011, 2016.

Gorum, T., Fan, X., van Westen, C. J., Huang, R., Xu, Q., Tang, C., and Wang G.: Distribution pattern of earthquake-induced landslides triggered by the 12 May 2008 Wenchuan earthquake, Geomorphology, 133, 152–167, doi: 10.1016/j.geomorph.2010.12.030, 2011.

Guo, X., Cui, P., Li, Y., Ma, L., Ge, Y., and Mahoney, W. B.: Intensity-duration threshold of rainfall-triggered debris flows in the Wenchuan Earthquake affected area, China, Geomorphology, 253, 208–216, doi: 10.1016/j.geomorph.2015.10.009, 2016.

Guo, X., Cui, P., Marchi, L., and Ge, Y.: Characteristics of rainfall responsible for debris flows in Wenchuan Earthquake area, Environmental Earth Sciences, 76, 596, doi: 10.1007/s12665-017-6940-y, 2017.

Guzzetti, F., Malamud, B. D., Turcotte, D. L., and Reichenbach, P.: Power-law correlations of landslide areas in Central Italy, Earth Planet. Sci. Lett., 195, 169–183, doi: 10.1016/S0012-821X(01)00589-1, 2002.

Guzzetti, F., Peruccacci, S., Rossi, M., and Stark, C. P.: Rainfall thresholds for the initiation of landslides in central and southern Europe, Meteorog. Atmos. Phys., 98, 239–267, doi: 10.1007/s00703-007-0262-7, 2007.

Guzzetti, F., Ardizzone, F., Cardinali, M., Rossi, M., and Valigi, D.: Landslide volumes and landslide mobilization rates in Umbria, central Italy, Earth Planet. Sci. Lett, 279, 222-229, doi: 10.1016/j.epsl.2009.01.005, 2009.

Guzzetti, F., Mondini, A. C., Cardinali, M., Fiorucci, F., Santangelo, M., and Chang, K.-T.: Landslide inventory maps: New tools for an old problem, Earth Sci. Rev., 112 (1-2), 42-66, doi: 10.1016/j.earscirev.2012.02.001, 2012.

Harp, E. L., Keefer, D. K., Sato, H. P., and Yagi, H.: Landslide inventories: the essential part of seismic landslide hazard analyses, Eng. Geol., 122 (1-2), 9-21, doi: 10.1016/j.enggeo.2010.06.013, 2011.

Hovius, N., Meunier, P., and Ching-weei, L.: Prolonged seismically induced erosion and the mass balance of a large earthquake, Earth Planet. Sci. Lett., 304, 347–355, doi: 10.1016/j.epsl.2011.02.005, 2011.

Hu, W., Scaringi, G., Xu, Q., Pei, G., van Asch, T. W. J., and Hicher, P. Y.: Sensitivity of the initiation and runout of flowslides in loose granular deposits to the content of small particles: An insight from flume tests, Eng. Geol., 231, 34-44, doi: 10.1016/j.enggeo.2017.10.001, 2017.

Hu, W., Hicher, P.-Y., Scaringi, G., Xu, Q., van Asch, T. W. J., and Wang, G.: Seismic precursor to instability induced by internal erosion in loose granular slopes, Géotechnique, doi: https://doi.org/10.1680/jgeot.17.P.079, 2018a.

Hu, W., Scaringi, G., Xu, Q., and Huang, R.: Acoustic emissions and micro-seismicity in granular slopes prior to failure and flow-like motion: The potential for early warning, Geophys. Res. Lett., doi: 10.1029/2018GL079724, 2018b.

Hu, W., Scaringi, G., Xu, Q., and Huang, R.: Internal Erosion Controls Failure and Runout of Loose Granular Deposits: Evidence From Flume Tests and Implications for Postseismic Slope Healing, Geophys. Res. Lett., 45 (11), 5518-5527, doi: 10.1029/2018GL078030, 2018c.

Huang, J., Huang, R., Ju, N., Xu, Q., and He, C.: 3D WebGIS platform for debris flow early warning: A case study, Eng. Geol., 197, 57-66, doi: 10.1016/j.enggeo.2015.08.013, 2015.

Huang, R., and Fan, X.: The landslide story, Nature Geosci., 6, 325–326, doi: 10.1038/ngeo1806, 2013.

Hungr, O., Leroueil, S., and Picarelli, L.: The Varnes classification of landslide types, an update, Landslides, 11 (2), 167-194, doi: 10.1007/s10346-013-0436-y, 2014.

Jakob, M., and Weatherly, H.: A hydroclimatic threshold for landslide initiation on the North Shore Mountains of Vancouver, British Columbia, Geomorphology, 54, 137–156, doi: 10.1016/S0169-555X(02)00339-2, 2003.

Jakob, M., Owen, T., and Simpson, T.: A regional real-time debris flow warning system for the District of North Vancouver, Canada, Landslides, 9, 165–178, doi: 10.1007/s10346-011-0282-8, 2012.

Kargel, J. S., Leonard, G. J., Shugar, D. H. et al.: Geomorphic and geologic controls of geohazards induced by Nepal's 2015 Gorkha earthquake, Science, 351 (6259), aac8353, doi: 10.1126/science.aac8353, 2016.

Keefer, D. K.: The importance of earthquake-induced landslides to long-term slope erosion and slope-failure hazards in seismically active regions, Geomorphology, 10, 265–284, doi: 10.1016/0169-555X(94)90021-3, 1994.

Keefer, D. K.: Investigating Landslides Caused by Earthquakes – A Historical Review, Surv. Geophys., 23 (6), 473-510, doi: 10.1023/A:1021274710840, 2002.

Kirschbaum, D., Adler, R., Hong, Y., Kumar, S., Peters-Lidard, C., and Lerner-Lam, A.: Advances in landslide nowcasting: evaluation of a global and regional modeling approach, Environ. Earth Sci., 66, 1683–1696, doi: 10.1007/s12665-011-0990-3, 2012.

Koi, T., Hotta, N., Ishigaki, I., Matuzaki, N., Uchiyama, Y., and Suzuki, M.: Prolonged impact of earthquake-induced landslides on sediment yield in a mountain watershed: The Tanzawa region, Japan, Geomorphology, 101, 692–702, doi: 10.1016/j.geomorph.2008.03.007, 2008.

Li, G., West, A. J., Densmore, A. L., Jin, Z., Parker, R. N., and Hilton, R. G.: Seismic mountain building: Landslides associated with the 2008 Wenchuan earthquake in the context of a generalized model for earthquake volume balance, Geochem. Geophys. Geosys., 15, 833–844, doi: 10.1002/2013GC005067, 2014.

Li, G., West, A. J., Densmore, A. L., Jing, Z., Zhang, F., Wang, J., Clark, M., and Hilton, R. G.: Earthquakes drive focused denudation along a tectonically active mountain front, Earth Planet. Sci. Lett., 472, 253-265, doi: 10.1016/j.epsl.2017.04.040, 2017.

Lin, C. W., Liu, S. H., Lee, S. Y., and Lu, C. C.: Impacts of the Chi-Chi earthquake on subsequent rainfall-induced landslides in central Taiwan, Eng. Geol., 86, 87-101, doi: 10.1016/j.enggeo.2006.02.010, 2006.

Lin, G. W., Chen, H., Hovius, N., Horng, M. J., Dadson, S., Meunier, P., and Lines, M.: Effects of earthquake and cyclone sequencing on landsliding and fluvial sediment transfer in a mountain catchment: Earth Surf. Proc. Land., 33, 1354-1373, doi: 10.1002/esp.1716, 2008.

Liu, J., Yong, Y., Xiaoqing, C., Jiankang, L., Xingzhang, C.: Characteristics and hazard prediction of large-scale debris flow of Xiaojia Gully in Yingxiu Town, Sichuan Province, China, Eng. Geol., 180, 55-67, doi: 10.1016/j.enggeo.2014.03.017, 2014.

Malamud, B. D., Turcotte, D. L., Guzzetti, F, Reichenbach, P.: Landslide inventories and their statistical properties, Earth Surface Processes Landforms, 29, 687–711, 2014.

Marc, O., and Hovius, N.: Amalgamation in landslide maps: effects and automatic detection, Nat. Hazards Earth Syst. Sci., 15, 723–733, doi: 10.5194/nhess-15-723-2015, 2015.

Marc, O., Hovius, N., Meunier, P., et al.: Transient changes of landslide rates after earthquakes, Geology, 43(10), 883-886, doi: 10.1130/G36961.1, 2015.

Marc, O., Hovius, N., and Meunier, P.: The mass balance of earthquakes and earthquake sequences, Geophys. Res. Lett., 43, 3708–3716, doi: 10.1002/2016GL068333, 2016a.

Marc, O., Hovius, N., Meunier, P., Gorum, T., and Uchida, T.: A seismologically consistent expression for the total area and volume of earthquake-triggered landsliding, J. Geophys. Res.-Earth, 121, 640–663, doi: 10.1002/2015JF003732, 2016b.

Marc, O., Meunier, P., and Hovius, N.: Prediction of the area affected by earthquake-induced landsliding based on seismological parameters, Nat. Hazards Earth Syst. Sci., 17, 1159-1175, doi: 10.5194/nhess-17-1159-2017, 2017.

Marc, O., Hovius, N., Meunier, P., et al.: Elevated Landslide Rates After Earthquakes: Coupling Geomorphological and Geophysical Data to Constrain Rock Damage and Healing. Proceedings of the 5th International Symposium on Mega Earthquake Induced Geo-disasters and Long Term Effects, Chengdu, China, 11-16 May, 2018.

Massey, C., Townsend, D., Rathie, E., et al.: Landslides Triggered by the 14 November 2016 Mw 7.8 Kaikoura Earthquake, New Zealand, B. Seismol. Soc. Am., 108 (3B), 1630-1648, doi: 10.1785/0120170305, 2018.

Meunier, P., Hovius, N., and Haines, J. A.: Topographic site effects and the location of earthquake induced landslides, Earth Planet. Sci. Lett. 275, 221–232, doi: 10.1016/j.epsl.2008.07.020, 2008.

Nikolopoulos, E. I., Crema, S., Marchi, L., Marra, F., Guzzetti, F., and Borga, M.: Impact of uncertainty in rainfall estimation on the identification of rainfall thresholds for debris flow occurrence, Geomorphology, 221, 286–297, doi: 10.1016/j.geomorph.2014.06.015, 2014..

Okamoto, T., Sakurai, M., Tsuchiya, S., Yoshimatsu, H., Ogawa, K., and Wang, G.: Secondary hazard associated with
5   coseismic landslides. In: K. Ugai et al. (eds), Earthquake-Induced Landslides, Springer, pp. 77-82, doi: 10.1007/978-3-642-32238-9_8, 2012.

Panziera, L., Germann, U., Gabella, M., and Mandapaka, P. V.: NORA—Nowcasting of Orographic Rainfall by means of Analogues, Q. J. R. Meteorol. Soc., 137, 2106–2123, doi: 10.1002/qj.878, 2011.

Parker, R. N., Densmore, A. L., Rosser, N. J., De Michele, M., Li, Y., Huang, R., Whadcoat, S., and Petley, D. N.: Mass
10   wasting triggered by the 2008 Wenchuan earthquake is greater than orogenic growth, Nature Geosci. 4, 449–452, doi: 10.1038/ngeo1154, 2011.

Parker, R. N., Hancox, G. T., Petley, D. N., et al.: Spatial distributions of earthquake-induced landslides and hillslope preconditioning in the northwest South Island, New Zealand, Earth Surf. Dyn., 3, 501-525, doi: 10.5194/esurf-3-501-2015, 2015.

15   Pawłuszek, K., Borkowski, A., and Tarolli, P.: Towards the optimal pixel size of DEM for automatic mapping of landslide areas. The International Archives of the Photogrammetry, Remote Sensing and Spatial Information Sciences, Vol. XLII-1/W1, 2017 ISPRS Hannover Workshop: HRIGI 17 – CMRT 17 – ISA 17 – EuroCOW 17, 6–9 June 2017, Hannover, Germany. https://doi.org/10.5194/isprs-archives-XLII-1-W1-83-2017, 2017.

Rossi, M., Kirschbaum, D., Luciani, S., Mondini, A. C., and Guzzetti, F.: TRMM satellite rainfall estimates for landslide early
20   warning in Italy: preliminary results. Proceedings of SPIE — The International Society for Optical Engineering, 8523, art. no. 85230D, 2012.

Qi, S., Xu, Q., Lan, H., Zhang, B., and Liu, J.: Spatial distribution analysis of landslides triggered by 2008.5.12 Wenchuan Earthquake, China, Eng. Geol., 116, 95-108, doi: 10.1016/j.enggeo.2010.07.011, 2010.

Saba, S. B., van der Meijde, M., and van der Werff, H.: Spatiotemporal landslide detection for the 2005 Kashmir earthquake
25   region, Geomorphology, 124, 17-25, doi: 10.1016/j.geomorph.2010.07.026, 2010.

Santangelo, M., Marchesini, I., and Bucci, M.: An approach to reduce mapping errors in the production of landslide inventory maps, Nat. Hazards Earth Syst. Sci., 15, 2111–2126, doi: 10.5194/nhess-15-2111-2015, 2015.

Scaringi, G., Fan, X., Xu, Q., Liu, C., Ouyang, C., Domènech, G., Yang, F., and Dai, L.: Some considerations on the use of numerical methods to simulate past landslides and possible new failures: the case of the recent Xinmo landslide (Sichuan,
30   China), Landslides, 15 (7), 1359-1375, doi: 10.1007/s10346-018-0953-9, 2018.

Schmitt, R. G., Tanyas, H., Nowicki Jessee, M. A., et al.: An open repository of earthquake-triggered ground-failure inventories: U.S. Geological Survey data release collection, doi: 10.5066/F7H70DB4, 2017.

Shieh, C. L., Chen, Y. S., Tsai, Y. J., and Wu, J. H.: Variability in rainfall threshold for debris flow after the Chi-Chi earthquake in central Taiwan, China, Int. J. Sediment. Res., 24, 177–188, doi: 10.1016/S1001-6279(09)60025-1, 2009.

Smith, R. B., Jiang, Q., Fearon, M. G., Tabary, P., Dorninger, M., Doyle, J. D., and Benoit, R.: Orographic precipitation and air mass transformation: an Alpine example, Q. J. R. Meteorol. Soc., 129, 433–454, doi: 10.1256/qj.01.212, 2003.

Stoffel, M., Bollschweiler, M., and Beniston, M.: Rainfall characteristics for periglacial debris flows in the Swiss Alps: past incidences—potential future evolutions, Clim. Chang., 105, 263–280, doi: 10.1007/s10584-011-0036-6, 2011.

Tang, C., Zhu, J., Li, W. L., and Liang, J. T.: Rainfall-triggered debris flows following the Wenchuan earthquake, Bull. Eng. Geol. Environ., 68 (2), 187-194, doi: 10.1007/s10064-009-0201-6, 2009.

Tang, C., Zhu, J., Ding, J., et al.: Catastrophic debris flows triggered by a 14 August 2010 rainfall at the epicenter of the Wenchuan earthquake, Landslides, 8, 485–497, doi: 10.1007/s10346-011-0269-5, 2011.

Tang, C., van Asch, T.W J., Chang, M., Chen, G. Q., Zhao, X. H., and Huang, X. C.: Catastrophic debris flows on 13 august 2010 in the Qingping area, southwestern china: the combined effects of a strong earthquake and subsequent rainstorms, Geomorphology 139, 559-576, doi: 10.1016/j.geomorph.2011.12.021, 2012.

Tang, C., van Westen, C. J., Tanyas, H., and Jetten, V. G.: Analysing post-earthquake landslide activity using multi-temporal landslide inventories near the epicentral area of the 2008 Wenchuan earthquake, Nat. Hazards Earth Syst. Sci. 16, 2641-2655, doi: 10.5194/nhess-16-2641-2016, 2016.

Tang, R., Fan, X., Scaringi, G., Xu, Q., van Westen, C. J., Ren, J., Havenith, H. B.: Distinctive controls on the distribution of river-damming and non-damming landslides induced by the 2008 Wenchuan earthquake, Bull. Eng. Geol. Environ., doi: 10.1007/s10064-018-1381-8, 2018.

Tanyas, H., van Westen, C. J., Allstadt, K. E., et al.: Presentation and Analysis of a Worldwide Database of Earthquake-Induced Landslide Inventories, J. Geophys. Res.-Earth, 122 (10), 1991-2015, doi: 10.1002/2017JF004236, 2017.

van Westen, C. J., van Asch, T. W. J, and Soeters, R.: Landslide hazard and risk zonation—why is it still so difficult?, Bull. Eng. Geol. Environ., 65, 167–184, doi: 10.1007/s10064-005-0023-0, 2006.

Wang, G., Huang, R., Lourenço, D. N., and Kamai, T.: A large landslide triggered by the 2008 Wenchuan (M8.0) earthquake in Donghekou area: Phenomena and mechanisms, Eng. Geol., 182, 148-157, doi: 10.1016/j.enggeo.2014.07.013, 2014.

Wang, J., Jin, Z., Hilton, R. G., et al.: Controls on fluvial evacuation of sediment from earthquake-triggered landslides, Geology, 43(2), 115-118, doi: 10.1130/G36157.1, 2015.

Wang, P., Zhang, B., Qiu, W., and Wang, J.: Soft-sediment deformation structures from the Diexi paleo-dammed lakes in the upper reaches of the Minjiang River, east Tibet, J. Asian Earth. Sci, 40 (4), 865-872, doi: 10.1016/j.jseaes.2010.04.006, 2011.

Wang, W., Godard, W., Liu-Zeng, J., et al.: Perturbation of fluvial sediments fluxes following the 2008 Wenchuan earthquake, Earth Surface Processes and Landforms, 42(15), 2611-2622, doi: 10.1002/esp.4210, 2017.

Xu, C., Xu, X., Yao, X., and Dai, F.: Three (nearly) complete inventories of landslides triggered by the May 12, 2008 Wenchuan Mw 7.9 earthquake of China and their spatial distribution statistical analysis, Landslides, 11, 441–461, doi: 10.1007/s10346-013-0404-6, 2014.

Xu, C., Xu, X., Lingling, S., et al.: Optimized volume models of earthquake-triggered landslides, Sci. Rep., 6, 29797, doi: 10.1038/srep29797, 2016.

Xu, Q., Zhang, S., Li, W. L., and Van Asch, T. W. J.: The 13 August 2010 catastrophic debris flows after the 2008 Wenchuan earthquake, China, Nat. Hazards Earth Syst. Sci., 12, 201–216, doi: 10.5194/nhess-12-201-2012, 2012.

5   Yang, W., Qi, W., Wang, M., et al.: Spatial and temporal analyses of post-seismic landslide changes near the epicentre of the Wenchuan earthquake, Geomorphology, 276, 8-15, doi: 10.1016/j.geomorph.2016.10.010, 2016.

Yang, W., Qi, W., and Zhou, J.: Decreased post-seismic landslides linked to vegetation recovery after the 2008 Wenchuan earthquake, Ecol. Eng., 89, 438-444, doi: 10.1016/j.ecolind.2017.12.006, 2018.

Yu, B., Ma, Y., and Wu, Y.: Investigation and study of debris flow disasters in Wenjiagou, Qingping Township, Mianzhu City,
10   Sichuan Province, Journal of Engineering Geology, 18 (6), 827-836, 2010 (in Chinese).

Yu, B., Wu, Y. F., and Chu, S. M.: Preliminary study of the effect of earthquakes on the rainfall threshold of debris flows. Eng. Geol., 182, 130–135, doi: 10.1016/j.enggeo.2014.04.007, 2014.

Zhang, S., and Zhang, L. M.: Impact of the 2008 Wenchuan earthquake in China on subsequent long-term debris flow activities in the epicentral area, Geomorphology, 276, 86–103, doi: 10.1016/j.geomorph.2016.10.009, 2017.

15   Zhang S, Zhang L. M., Chen H. X.: Relationships among three repeated large-scale debris flows at Pubugou Ravine in the Wenchuan earthquake zone, Can. Geotech. J., 51, 951–965, doi: 10.1139/cgj-2013-0368, 2014.

Zhang, S., Zhang, L., Lacasse, S., and Nadim, F.: Evolution of Mass Movements near Epicentre of Wenchuan Earthquake, the First Eight Years, Sci. Rep., 6, 36154, doi: 10.1038/srep36154, 2016.